

A comparison of different order hybrid finite difference-volume for the Serre equations in conservative form

Jordan Pitt,¹ Not a Member, ASCE
Christopher Zoppou,¹ Member, ASCE
Stephen G. Roberts,¹ Not a Member, ASCE

ABSTRACT

Keywords: dispersive waves, conservation laws, Serre equation, shallow water wave equations, finite volume method, finite difference method

¹ INTRODUCTION

² [credit derivars]

³ SERRE EQUATIONS

⁴ The Serre equations can derived as an approximation to the full Euler equations by
⁵ depth integration similar to (Su and Gardner 1969). They can also be seen as an asymptotic
⁶ expansion to the Euler equations as well (Lannes and Bonneton 2009). The former is more
⁷ consistent with the perspective from which numerical methods will be developed while the
⁸ latter indicates the appropriate regions in which to use these equations as a model for fluid
⁹ flow. The set up of the scenario under which the Serre approximation is made consists
¹⁰ of a 2 dimensional $\mathbf{x} = (x, z)$ fluid over a bottom topography as in Figure 1 acting under
¹¹ gravity. Consider a fluid particle at depth $\xi(\mathbf{x}, t) = z - h(x, t) - z_b(x)$ below the water
¹² surface, see Figure 1. Where the water depth is $h(x, t)$ and $z_b(x)$ is the bed elevation. The
¹³ fluid particle is subject to the pressure, $p(\mathbf{x}, t)$ and gravitational acceleration, $\mathbf{g} = (0, g)^T$
¹⁴ and has a velocity $\mathbf{u} = (u(\mathbf{x}, t), w(\mathbf{x}, t))$, where $u(\mathbf{x}, t)$ is the velocity in the x -coordinate and
¹⁵ $w(\mathbf{x}, t)$ is the velocity in the z -coordinate and t is time. Assuming that $z_b(x)$ is constant the
¹⁶ Serre equations read (Li et al. 2014)

$$\frac{\partial h}{\partial t} + \frac{\partial(\bar{u}h)}{\partial x} = 0 \quad (1a)$$

$$\underbrace{\frac{\partial(\bar{u}h)}{\partial t} + \frac{\partial}{\partial x} \left(\bar{u}^2 h + \frac{gh^2}{2} \right)}_{\text{Shallow Water Wave Equations}} + \underbrace{\frac{\partial}{\partial x} \left(\frac{h^3}{3} \left[\frac{\partial \bar{u}}{\partial x} \frac{\partial \bar{u}}{\partial x} - \bar{u} \frac{\partial^2 \bar{u}}{\partial x^2} - \frac{\partial^2 \bar{u}}{\partial x \partial t} \right] \right)}_{\text{Dispersion Terms}} = 0. \quad (1b)$$

Serre Equations

¹Mathematical Sciences Institute, Australian National University, Canberra, ACT 0200, Australia, E-mail: Jordan.Pitt@anu.edu.au. The work undertaken by the first author was supported financially by an Australian National University Postgraduate Research Award.

22 Where \bar{u} means the average of u over the depth of water.

23 **Alternative Conservation Law Form of the Sere Equations**

24 In (Le Métayer et al. 2010; Li et al. 2014) it is demonstrated that the Serre equations
25 can be rearranged into a conservation law form, by the addition of a new quantity G .

26
$$G = uh - h^2 \frac{\partial h}{\partial x} \frac{\partial u}{\partial x} - \frac{h^3}{3} \frac{\partial^2 u}{\partial x^2}. \quad (2)$$

27

28 Consequently the equations can be rewritten as

29
$$\frac{\partial h}{\partial t} + \frac{\partial(uh)}{\partial x} = 0, \quad (3a)$$

30
31

32
$$\frac{\partial G}{\partial t} + \frac{\partial}{\partial x} \left(Gu + \frac{gh^2}{2} - \frac{2h^3}{3} \frac{\partial u}{\partial x} \frac{\partial u}{\partial x} \right) = 0. \quad (3b)$$

33

34 Where the bar over u has been dropped for ease of notation. This opens the Serre equations
35 up to a hybrid method that for each time step solves the elliptic problem (2) for u and then
36 the conservation law (3) with a finite volume method. As was done in (Le Métayer et al.
37 2010).

38 **NUMERICALLY SOLVING THE SERRE EQUATIONS WRITTEN IN
39 CONSERVATION LAW FORM**

40 There are numerous ways a numerical method could be built to solve the Serre equa-
41 tions, in this form and allowing for discontinuities a finite volume method seems the most
42 appropriate. Such a method can now be applied due to the rearranging of the equations
43 performed above. However, it can only handle the equation (3), to show how (2) can also
44 be used some notation will be introduced. Consider a discretisation in time that will be
45 denoted by superscript, for instance $h^n \approx h(x, t^n)$. Now consider a finite volume method to
46 solve (3) that is any order in space and time; it updates the conserved quantities h and G
47 from time t^n to t^{n+1} . Such a method would act like so

48
$$\begin{bmatrix} h^{n+1} \\ G^{n+1} \end{bmatrix} = \mathcal{L}(h^n, G^n, u^n, \Delta t). \quad (4)$$

49

50 Where \mathcal{L} is the numerical solver for (3) that does a single time step Δt . Clearly it can be
51 seen that in addition to \mathcal{L} another method is required that solves for u^n from h^n and G^n .
52 Indeed using a numerical method to solve for u in (2) using h and G would give such a
53 method, it would act like so

54
$$u = \mathcal{A}(h, G). \quad (5)$$

55

56 Thus given h^n and G^n a time step that gives these conserved quantities at t^{n+1} is given by:

57 $u^n = \mathcal{A}(h^n, G^n),$

59

60
$$\begin{bmatrix} h^{n+1} \\ G^{n+1} \end{bmatrix} = \mathcal{L}(h^n, G^n, u^n, \Delta t).$$

62 Where \mathcal{L} can be a finite volume method because of the rearrangement of the equations and
63 can thus handle discontinuities in the conserved variables.

64 **METHOD FOR \mathcal{A}**

65 In the above section a very general map of a typical time step in these hybrid methods
66 for the Serre equations and a discretisation in time were given. In this paper a fully discrete
67 system will be built hence a discretisation of space is also introduced, denoted by subscript
68 i for example $h_i^n \approx h(x_i, t^n)$. Additionally assume that this discretisation in space is fixed
69 so that $\forall i x_{i+1} - x_i = \Delta x$. For a fixed time (2) is just an ordinary differential equation,
70 thus it seems reasonable that solving a finite difference approximation of it would give a
71 satisfactory method for \mathcal{A} . Since the goal of this paper is to develop and compare a
72 range of different order methods for this problem both a second- and fourth-order centred
73 finite difference approximation will be given for (2). These are approximations are as
74 follows

75
$$\left(\frac{\partial h}{\partial x} \right)_i = \frac{h_{i+1} - h_{i-1}}{2\Delta x}, \quad (6)$$

76

77
$$\left(\frac{\partial h}{\partial x} \right)_i = \frac{-h_{i+2} + 8h_{i+1} - 8h_{i-1} + h_{i-2}}{12\Delta x}, \quad (7)$$

80 which are second- and fourth-order in space respectively. Likewise a second- and fourth-
81 order central finite difference is applied to the double space derivative respectively

82
$$G_i = u_i h_i - h_i^2 \left(\frac{h_{i+1} - h_{i-1}}{2\Delta x} \right) \left(\frac{u_{i+1} - u_{i-1}}{2\Delta x} \right) - \frac{h_i^3}{3} \left(\frac{u_{i+1} - 2u_i + u_{i-1}}{\Delta x^2} \right), \quad (8)$$

83

84
$$G_i = u_i h_i - h_i^2 \left(\frac{-h_{i+2} + 8h_{i+1} - 8h_{i-1} + h_{i-2}}{12\Delta x} \right) \left(\frac{-u_{i+2} + 8u_{i+1} - 8u_{i-1} + u_{i-2}}{12\Delta x} \right) - \frac{h_i^3}{3} \left(\frac{-u_{i+2} + 16u_{i+1} - 30u_i + 16u_{i-1} - u_{i-2}}{12\Delta x^2} \right). \quad (9)$$

85

86

87 Both of these can be rearranged into a matrix equation with the following form

88

$$\begin{bmatrix} G_0 \\ \vdots \\ G_m \end{bmatrix} = A \begin{bmatrix} u_0 \\ \vdots \\ u_m \end{bmatrix}.$$

89

90 For a second-order approximation the matrix A is tri-diagonal while for a fourth-order
91 scheme A is penta-diagonal. Thus for both cases A has the following form

92

$$A = \begin{bmatrix} c_0 & d_0 & e_0 & 0 & \cdots & \cdots & \cdots & \cdots & 0 \\ b_1 & c_1 & d_1 & e_1 & 0 & \cdots & \cdots & \cdots & 0 \\ a_2 & b_2 & c_2 & d_2 & e_2 & 0 & \cdots & \cdots & 0 \\ 0 & a_3 & b_3 & c_3 & d_3 & e_3 & 0 & \cdots & 0 \\ \vdots & \ddots & \vdots \\ 0 & \cdots & 0 & a_{m-3} & b_{m-3} & c_{m-3} & d_{m-3} & e_{m-3} & 0 \\ 0 & \cdots & \cdots & 0 & a_{m-2} & b_{m-2} & c_{m-2} & d_{m-2} & e_{m-2} \\ 0 & \cdots & \cdots & \cdots & 0 & a_{m-1} & b_{m-1} & c_{m-1} & d_{m-1} \\ 0 & \cdots & \cdots & \cdots & \cdots & 0 & a_m & b_m & c_m \end{bmatrix}$$

93

Where for the second-order scheme these are given by

$$a_i = 0, \quad (10a)$$

$$b_i = \frac{h_i^2}{2\Delta x} \frac{h_{i+1} - h_{i-1}}{2\Delta x} - \frac{1}{3\Delta x^2} h_i^3, \quad (10b)$$

$$c_i = h_i + \frac{2h_i^3}{3\Delta x^2}, \quad (10c)$$

$$d_i = -\frac{h_i^2}{2\Delta x} \frac{h_{i+1} - h_{i-1}}{2\Delta x} - \frac{1}{3\Delta x^2} h_i^3, \quad (10d)$$

$$e_i = 0. \quad (10e)$$

While for a fourth-order scheme these are given by

$$a_i = -\left(\frac{-h_{i+2} + 8h_{i+1} - 8h_{i-1} + h_{i-2}}{144\Delta x^2} \right) h_i^2 + \frac{h_i^3}{36\Delta x^2}, \quad (11a)$$

$$b_i = 8 \left(\frac{-h_{i+2} + 8h_{i+1} - 8h_{i-1} + h_{i-2}}{144\Delta x^2} \right) h_i^2 + 16 \frac{h_i^3}{36\Delta x^2}, \quad (11b)$$

$$c_i = h_i + \frac{30h_i^3}{36\Delta x^2}, \quad (11c)$$

$$d_i = -8 \left(\frac{-h_{i+2} + 8h_{i+1} - 8h_{i-1} + h_{i-2}}{144\Delta x^2} \right) h_i^2 + 16 \frac{h_i^3}{36\Delta x^2}, \quad (11d)$$

$$e_i = \left(\frac{-h_{i+2} + 8h_{i+1} - 8h_{i-1} + h_{i-2}}{144\Delta x^2} \right) h_i^2 + \frac{h_i^3}{36\Delta x^2}. \quad (11e)$$

94 Then

$$95 \quad \mathcal{A} := A^{-1} \begin{bmatrix} G_0^n \\ \vdots \\ G_m^n \end{bmatrix},$$

96 Where A will also use values at time t^n . Furthermore \mathcal{A}_2 and \mathcal{A}_4 will refer to the second-
97 and fourth-order version of this respectively. Thus a satisfactory order method in space
98 has been devised to solve the elliptic problem (2) in the Serre equations.

100 METHOD FOR \mathcal{L}

101 A finite volume method of sufficient order was developed to solve (3). Importantly
102 finite volumes have a different discretion of space, so a new notation is introduced which
103 will now be demonstrated by example

$$104 \quad \bar{h}_i = \frac{1}{\Delta x} \int_{x_{i-\frac{1}{2}}}^{x_{i+\frac{1}{2}}} h(x, t) dx.$$

105 Where $x_{i\pm\frac{1}{2}} = x_i \pm \frac{\Delta x}{2}$. Finite volume schemes work with these cell averaged values and
106 give them as outputs by the following scheme

$$108 \quad \bar{U}_i^{n+1} = \bar{U}_i^n - \frac{\Delta t}{\Delta x} \left(\mathbf{F}_{i+\frac{1}{2}}^n - \mathbf{F}_{i-\frac{1}{2}}^n \right).$$

109 Where \bar{U}_i^n is an approximation of the vector of the conserved quantities averaged over the
110 cell at time t^n while $\mathbf{F}_{i\pm\frac{1}{2}}^n$ is an approximation of the average flux at $x_{i\pm\frac{1}{2}}$ over the time
111 interval $[t^n, t^{n+1}]$ given by approximating the Riemann problem at the cell boundaries. The
112 values to the left and right of a cell edge say $x_{i+\frac{1}{2}}$ are reconstructed by assuming appropriate
113 order polynomials over each cell. For example for h this would result in $h_{i+\frac{1}{2}}^-$ and $h_{i+\frac{1}{2}}^+$ for
114 the left and right reconstructed values at $x_{i+\frac{1}{2}}$.

116 *Reconstruction*

117 The order of the polynomials used to reconstruct the quantities inside the cell deter-
 118 mines the order of the scheme in space. In Godunov's original formulation of the method
 119 [] the polynomials are constant functions resulting in a first order method. Similarly first-
 120 and second-degree polynomials result in second- and third-order schemes. To make this
 121 section easier the following notation is introduced P_i^k denotes the polynomial of degree k
 122 for any quantity q over the interval with x_i as its midpoint. Thus for a 0-degree polynomial
 123 the reconstruction formula is

$$124 \quad P_i^0 = \bar{q}_i = q_i. \quad (12)$$

126 However for higher degree polynomials the extra degrees of freedom mean that choices
 127 have to be made to decide the behaviour of the fitted polynomial. For linear functions the
 128 midpoint of a quantity on an interval and the average of the quantity over the interval are
 129 the same. Thus the natural choice for the slope of P_i^1 is the slope between the midpoints
 130 of the two neighbouring cells. While for third-order it is reasonable to use the degrees of
 131 freedom so that the polynomial has the correct average value over its corresponding cell
 132 and its two neighbours either side. However to suppress non-physical oscillations limiting
 133 must be implemented. For the second-order scheme the minmod limiter was used as in
 134 (Kurganov et al. 2002), while for the third-order scheme the Koren limiter was used(Koren
 135 1993). This results in the following fitting schemes respectively

$$136 \quad P_i(x) = a_i(x - x_i) + q_i, \quad (13a)$$

$$139 \quad a_i = \text{minmod} \left\{ \theta \frac{q_{i+1} - q_i}{\Delta x}, \frac{q_{i+1} - q_{i-1}}{2\Delta x}, \theta \frac{q_i - q_{i-1}}{\Delta x} \right\} \quad \text{for } \theta \in [1, 2] \quad (13b)$$

$$141 \quad r_i = \frac{\bar{q}_{i+1} - \bar{q}_i}{\bar{q}_i - \bar{q}_{i-1}} \quad (14a)$$

$$143 \quad q_{i+\frac{1}{2}}^- = \bar{q}_i + \frac{1}{2} \phi^-(r_i) (\bar{q}_i - \bar{q}_{i-1}) \quad (14b)$$

$$145 \quad q_{i+\frac{1}{2}}^+ = \bar{q}_i - \frac{1}{2} \phi^+(r_i) (\bar{q}_i - \bar{q}_{i-1}) \quad (14c)$$

$$147 \quad \phi^-(r_i) = \max \left[0, \min \left[2r_i, \frac{1+2r_i}{3}, 2 \right] \right] \quad (14d)$$

$$149 \quad \phi^+(r_i) = \max \left[0, \min \left[2r_i, \frac{2+r_i}{3}, 2 \right] \right] \quad (14e)$$

151 *Local Riemann Problem*

152 Since \bar{U}_i^n what remains in the equations is to calculate the two fluxes. As stated above
 153 this is done by approximating the Riemann problem, in (Kurganov et al. 2002) the follow-
 154 ing formula is derived

$$155 \quad F_{i+\frac{1}{2}} = \frac{a_{i+\frac{1}{2}}^+ f\left(q_{i+\frac{1}{2}}^-\right) - a_{i+\frac{1}{2}}^- f\left(q_{i+\frac{1}{2}}^+\right)}{a_{i+\frac{1}{2}}^+ - a_{i+\frac{1}{2}}^-} + \frac{a_{i+\frac{1}{2}}^+ a_{i+\frac{1}{2}}^-}{a_{i+\frac{1}{2}}^+ - a_{i+\frac{1}{2}}^-} \left[q_{i+\frac{1}{2}}^+ - q_{i+\frac{1}{2}}^- \right]. \quad (15)$$

156 Where f is just the flux function of the conservative law for quantity q . While $a_{i+\frac{1}{2}}^+$ and
 $a_{i+\frac{1}{2}}^-$ are given by

$$157 \quad a_{i+\frac{1}{2}}^+ = \max \left[\lambda_2 \left(q_{i+\frac{1}{2}}^- \right), \lambda_2 \left(q_{i+\frac{1}{2}}^+ \right), 0 \right], \quad (16a)$$

$$158 \quad a_{i+\frac{1}{2}}^- = \min \left[\lambda_1 \left(q_{i+\frac{1}{2}}^- \right), \lambda_1 \left(q_{i+\frac{1}{2}}^+ \right), 0 \right]. \quad (16b)$$

159 Where λ_1 and λ_2 are estimates of the smallest and largest eigenvalues respectively of the
 160 Jacobian which corresponds to the phase speeds.

161 *Propagation Speeds of a Local Shock*

162 As demonstrated in (Le Métayer et al. 2010) [] the phase speeds are bounded from
 163 above and below by the phase speed of the Shallow Water Wave Equations, so that

$$164 \quad \lambda_1 := u - \sqrt{gh} \leq v_p \leq u + \sqrt{gh} =: \lambda_2. \quad (17)$$

165 Thus $a_{i+\frac{1}{2}}^+$ and $a_{i+\frac{1}{2}}^-$ are fully determined.

166 *Fully discrete approximations to flux function*

167 For height the fully discrete any order approximation to $f(h_{i+\frac{1}{2}}^-)$ and $f(h_{i+\frac{1}{2}}^+)$ are clear
 168 and given by

$$169 \quad f \left(h_{i+\frac{1}{2}}^- \right) = u_{i+\frac{1}{2}}^- h_{i+\frac{1}{2}}^-, \quad (18a)$$

$$170 \quad f \left(h_{i+\frac{1}{2}}^+ \right) = u_{i+\frac{1}{2}}^+ h_{i+\frac{1}{2}}^+. \quad (18b)$$

173 For G this is complicated by derivative, leaving in place a general approximation derivative
 174 it looks like so

$$175 \quad f\left(G_{i+\frac{1}{2}}^{-}\right) = u_{i+\frac{1}{2}}^{-} G_{i+\frac{1}{2}}^{-} + \frac{g\left(h_{i+\frac{1}{2}}^{-}\right)^2}{2} - \frac{2\left(h_{i+\frac{1}{2}}^{-}\right)^3}{3} \left[\left(\frac{\partial u}{\partial x} \right)_{i+\frac{1}{2}}^{-} \right]^2, \quad (19a)$$

176

177

$$178 \quad f\left(G_{i+\frac{1}{2}}^{+}\right) = u_{i+\frac{1}{2}}^{+} G_{i+\frac{1}{2}}^{+} + \frac{g\left(h_{i+\frac{1}{2}}^{+}\right)^2}{2} - \frac{2\left(h_{i+\frac{1}{2}}^{+}\right)^3}{3} \left[\left(\frac{\partial u}{\partial x} \right)_{i+\frac{1}{2}}^{+} \right]^2. \quad (19b)$$

180 There are multiple ways to approximate this derivative with different corresponding orders
 181 of accuracy. The first- and third-order approximations are the most natural and come
 182 from upwind finite difference approximations [] while the second-order choice is an intuitive
 183 choice that has the correct order and is simpler to implement than its upwind finite
 184 difference approximation. Thus there are the following approximations to the derivatives

$$185 \quad \left(\frac{\partial u}{\partial x} \right)_{i+\frac{1}{2}}^{+} = \frac{u_{i+\frac{3}{2}}^{+} - u_{i+\frac{1}{2}}^{+}}{\Delta x}, \quad (20a)$$

186

187

$$188 \quad \left(\frac{\partial u}{\partial x} \right)_{i+\frac{1}{2}}^{-} = \frac{u_{i+\frac{1}{2}}^{-} - u_{i-\frac{1}{2}}^{-}}{\Delta x}, \quad (20b)$$

189

190

$$191 \quad \left(\frac{\partial u}{\partial x} \right)_{i+\frac{1}{2}}^{-} = \left(\frac{\partial u}{\partial x} \right)_{i+\frac{1}{2}}^{+} = \frac{u_{i+1} - u_i}{\Delta x}, \quad (21)$$

192

193

$$194 \quad \left(\frac{\partial u}{\partial x} \right)_{i+\frac{1}{2}}^{+} = \frac{-u_{i+\frac{3}{2}}^{+} + 4u_{i+\frac{3}{2}}^{+} - 3u_{i+\frac{1}{2}}^{+}}{\Delta x}, \quad (22a)$$

195

196

$$197 \quad \left(\frac{\partial u}{\partial x} \right)_{i+\frac{1}{2}}^{-} = \frac{3u_{i+\frac{1}{2}}^{-} - 4u_{i-\frac{1}{2}}^{-} + u_{i-\frac{3}{2}}^{-}}{\Delta x} \quad (22b)$$

198 For the first-, second- and third-order schemes respectively.

200 Transforming between midpoints and averages

Notice that the schemes for \mathcal{L} uses cell averages and values at the cell boundaries based on the reconstruction. While \mathcal{A} uses fixed points at the cell centres, thus between applying the two schemes a transformation from the cell averages to the cell centres must be made. For the first- and second-order schemes this distinction is trivial since $\bar{q}_i = q_i$ so both operations work with the same values. However for third-order schemes this is a very important distinction and failure to handle this will result in a loss of accuracy. For this problem it is enough to go back to the intuitive quadratic polynomial to fit on the interval centred at x_i so that the polynomial also gives the correct cell averages for the two neighbouring cells. This results in the following

$$q_i = \frac{-\bar{q}_{i+1} + 26\bar{q}_i - \bar{q}_{i-1}}{24}. \quad (23)$$

212 Thus one can form a matrix equation between the vector of all midpoint values and all
 213 cell average values and use the resultant transformation matrix to go back and forth. For
 214 convenience denote the transformation from midpoints to cell averages by \mathcal{M} while the
 215 inverse matrix operation transforming from cell averages to midpoints will be denoted by
 216 \mathcal{M}^{-1} . This completes the effort to build a single time step for the system denoted by \mathcal{H} of
 217 equations which is now as follows

$$\begin{bmatrix} \mathbf{h}^n \\ \mathbf{G}^n \end{bmatrix} = \begin{bmatrix} \mathcal{M}^{-1}(\bar{\mathbf{h}}^n) \\ \mathcal{M}^{-1}(\bar{\mathbf{G}}^n) \end{bmatrix}$$

$$\mu^n \equiv \mathcal{A}(h^n, G^n),$$

$$\begin{bmatrix} \bar{\mathbf{h}}^n \\ \bar{\mathbf{G}}^n \\ \bar{\mathbf{u}}^n \end{bmatrix} = \begin{bmatrix} \mathcal{M}(\mathbf{h}^n) \\ \mathcal{M}(\mathbf{G}^n) \\ \mathcal{M}(\mathbf{u}^n) \end{bmatrix}$$

$$\left[\begin{array}{c} \bar{\boldsymbol{h}}^{n+1} \\ \bar{\boldsymbol{G}}^{n+1} \end{array} \right] = \mathcal{L}(\bar{\boldsymbol{h}}^n, \bar{\boldsymbol{G}}^n, \bar{\boldsymbol{u}}^n, \Delta t).$$

229 Strong-Stability-Preserving Runge-Kutta Scheme

²³⁰ The time step above is first order accurate there are many methods to increase the
²³¹ accuracy of such a method in time, this paper will follow the SSP RK steps as in (Gottlieb
²³² et al. 2009) to allow for fully second- and third-order schemes. These are constructed by

233 doing more of the time steps \mathcal{H} and then preforming a linear combinations of them. This
 234 leads to the following schemes for first-, second- and third- order time stepping schemes
 235 respectively

$$236 \quad \begin{bmatrix} \bar{\mathbf{h}}^{n+1} \\ \bar{\mathbf{G}}^{n+1} \end{bmatrix} = \mathcal{H}(\bar{\mathbf{h}}^n, \bar{\mathbf{G}}^n, \Delta t), \quad (24)$$

$$239 \quad \begin{bmatrix} \bar{\mathbf{h}}' \\ \bar{\mathbf{G}}' \end{bmatrix} = \mathcal{H}(\bar{\mathbf{h}}^n, \bar{\mathbf{G}}^n, \Delta t) \quad (25a)$$

$$242 \quad \begin{bmatrix} \bar{\mathbf{h}}'' \\ \bar{\mathbf{G}}'' \end{bmatrix} = \mathcal{H}(\bar{\mathbf{h}}', \bar{\mathbf{G}}', \Delta t) \quad (25b)$$

$$245 \quad \begin{bmatrix} \bar{\mathbf{h}}^{n+1} \\ \bar{\mathbf{G}}^{n+1} \end{bmatrix} = \frac{1}{2} \left(\begin{bmatrix} \bar{\mathbf{h}}^n \\ \bar{\mathbf{G}}^n \end{bmatrix} + \begin{bmatrix} \bar{\mathbf{h}}'' \\ \bar{\mathbf{G}}'' \end{bmatrix} \right), \quad (25c)$$

$$248 \quad \begin{bmatrix} \bar{\mathbf{h}}^{(1)} \\ \bar{\mathbf{G}}^{(1)} \end{bmatrix} = \mathcal{H}(\bar{\mathbf{h}}^n, \bar{\mathbf{G}}^n, \Delta t) \quad (26a)$$

$$251 \quad \begin{bmatrix} \bar{\mathbf{h}}^{(2)} \\ \bar{\mathbf{G}}^{(2)} \end{bmatrix} = \mathcal{H}(\bar{\mathbf{h}}^{(1)}, \bar{\mathbf{G}}^{(1)}, \Delta t) \quad (26b)$$

$$254 \quad \begin{bmatrix} \bar{\mathbf{h}}^{(3)} \\ \bar{\mathbf{G}}^{(3)} \end{bmatrix} = \frac{3}{4} \begin{bmatrix} \bar{\mathbf{h}}^n \\ \bar{\mathbf{G}}^n \end{bmatrix} + \frac{1}{4} \begin{bmatrix} \bar{\mathbf{h}}^{(2)} \\ \bar{\mathbf{G}}^{(2)} \end{bmatrix}, \quad (26c)$$

$$257 \quad \begin{bmatrix} \bar{\mathbf{h}}^{(4)} \\ \bar{\mathbf{G}}^{(4)} \end{bmatrix} = \mathcal{H}(\bar{\mathbf{h}}^{(3)}, \bar{\mathbf{G}}^{(3)}, \Delta t) \quad (26d)$$

$$260 \quad \begin{bmatrix} \bar{\mathbf{h}}^{(n+1)} \\ \bar{\mathbf{G}}^{(n+1)} \end{bmatrix} = \frac{1}{3} \begin{bmatrix} \bar{\mathbf{h}}^n \\ \bar{\mathbf{G}}^n \end{bmatrix} + \frac{2}{3} \begin{bmatrix} \bar{\mathbf{h}}^{(4)} \\ \bar{\mathbf{G}}^{(4)} \end{bmatrix}, \quad (26e)$$

263 **NUMERICAL SIMULATIONS**

264 The discussed methods will now be used to solve 3 different situations; analytic so-
 265 lution of the Serre equations given by the soliton, one of the experiments conducted by
 266 Segur and Hammack in (Hammack and Segur 1978) and finally a dambreak problem from
 267 (El et al. 2006; Le Métayer et al. 2010). The first two will be for validation reasons with
 268 the first being to validate whether the scheme reproduce the soliton and the order of con-
 269 vergence while the second validates the behaviour of a shock against experimental data.
 270 Lastly the dambreak will further look at how the scheme handles shocks.

271 **Soliton**

272 Currently there is only one family of analytic solutions to the Serre equations which
 273 are cnoidal waves (Carter and Cienfuegos 2011). This solution has been used to verify the
 274 order of convergence of the proposed methods in this paper, in particular for the soliton
 275 case of this family. Solitons travel without deformation and in the Serre equations they
 276 have the following form

277
$$h(x, t) = a_0 + a_1 \operatorname{sech}^2(\kappa(x - ct)), \quad (27a)$$

279

280
$$u(x, t) = c \left(1 - \frac{a_0}{h(x, t)} \right), \quad (27b)$$

281

282
$$\kappa = \frac{\sqrt{3a_1}}{2a_0 \sqrt{a_0 + a_1}}, \quad (27c)$$

283

284
$$c = \sqrt{g(a_0 + a_1)}. \quad (27d)$$

285
 286 Where a_0 and a_1 are input parameters that determine the depth of the quiescent water and
 287 the maximum height of the soliton above that respectively. For the conducted simulation
 288 $a_0 = 10m$, $a_1 = 1m$ over an x domain $[-500m, 1500m]$ from time $[0s, 100s]$. Where
 289 $\Delta t = \lambda \Delta x$ and $\lambda = 0.01$. For second-order $\theta = 1.2$. The example results for $\Delta x = 1.5625m$
 290 can be seen in figures 3-5, while the relative error as measured by the L1-norm of the
 291 method can be seen in figure 2.

292 Firstly figure 2 demonstrates that the schemes all have the correct order of convergence
 293 in both time and space since $\Delta t = \lambda \Delta x$ as desired. Clearly this order of convergence is not
 294 over all Δx the reason for this when Δx is large is that the actual problem is not discretised
 295 well at all since the cells are too large to represent the simulation properly and hence the
 296 order of convergence there will be significantly lower this can be seen for all sub-figures of

299 figure 2. For figure 2(c) there is also a decrease in the order of convergence this is because
300 the third-order scheme has become accurate enough for the floating point errors to become
301 significant, thus the behaviour of the order of convergence for all methods is as good as
302 one can expect.

303 Figures 3-5 demonstrate the superiority of the second- and third-order to the first-
304 order method. This can also be seen in 2 with the Δx required to produce an error of
305 the same magnitude for the second- and third-order methods is much smaller for the first-
306 order method. By inspecting the trailing edge of the soliton it can be seen that indeed as
307 expected and supported by figure 2 the third-order is better than the second-order method.
308 With graphical inspection showing the third-analytic solution to be identical on a relatively
309 coarse grid with less than 500 cells representing the actual soliton.

310 Because of the added complexity of the higher order methods they do require more
311 computational effort and hence are slower.[.] Although the superior error does overcome
312 this inefficiency.[.]

313 Segur Laboratory Experiment

314 In (Hammack and Segur 1978) Hammack and Segur conducted an experiment that
315 produced rectangular waves with the stroke of a $0.61m$ long piston flush with the wall of
316 a wavetank $31.6m$ long and recorded the wave heights at certain positions over time. The
317 quiescent water height h_1 was $0.1m$ while the stroke of the piston caused a depression of
318 water h_0 $0.095m$ deep. To run this as a numerical simulation the reflected problem must
319 be used, the result of this is that the simulation is reflected around the origin and $h_1 - h_0$ is
320 doubled by changing h_0 . Thus the domain is from $-60m$ to $60m$ and the simulation is run
321 for $50s$ with $\Delta x = 0.01$, $\lambda = \frac{0.2}{\sqrt{gh_1}}$ and $\theta = 1.2$. The results of this simulation are displayed
322 in figures 6 - 8.

323 In this experiment the initial depression causes a right going rarefaction fan and a left
324 going shock at least on the positive axis. The two shocks then reflect in the middle and so
325 the shock and the rarefaction fan are travelling in the same direction. The leading wave
326 in all the related figures is that rarefaction fan while the trailing dispersive waves are the
327 result of the reflected shock. The most important result of such a test is to investigate if
328 the period of the produced waves are coherent with the experiment. Because things such
329 as the wave heights, the number of waves and the speed of the waves will be different
330 because real water has effects that the model ignores.

331 From all the related figures it can be seen that all models show good agreement be-
332 tween the arrival of the first wave and the period of all the waves. While figure 6 shows
333 the first-order model is too diffusive and thus under approximates the wave heights of the
334 dispersive waves of the shock. While the second- and third-order methods over approx-
335 imate them. This discrepancy can be explained by the Serre equations not taking into

336 account viscous effects that diffuse the dispersive waves and so the Serre equations are
 337 actually producing an upper bound on the wave heights for fluids with viscosity. These
 338 experiments do validate the numerical schemes to correctly handle discontinuities. Also it
 339 demonstrates that the oscillations produced by the schemes are not non-physical.

340 **Dam-break**

341 The dam break problem can be defined as such

$$342 \quad h(x, 0) = \begin{cases} h_0 & x < x_m \\ h_1 & x \geq x_m \end{cases}, \quad (28)$$

343

344

$$345 \quad u(x, 0) = 0.0m/s. \quad (29)$$

347 For this problem the x domain was $[0m, 1000m]$ while the simulation was run until $t = 30s$.
 348 The other values were $h_0 = 1.8m$, $h_1 = 1.0m$, $x_m = 500m$, $\lambda = 0.01$ and $\theta = 1.2$.
 349 This corresponds to sub-critical flow and was a situation demonstrated in (El et al. 2006;
 350 Le Métayer et al. 2010). An example was plotted for $\Delta x = 0.09765625m$ for all the
 351 methods described in figure 10. To determine if the oscillations that occur in the solution
 352 indeed converge to some limit as $\Delta x \rightarrow 0$ multiple Δx values must be used and then the
 353 amount of variation in the solution measured. A common way to measure this is the total
 354 variation TV (LeVeque 2002) which for a vector v of length k is given by

$$355 \quad TV(v) = \sum_{\forall i>1} |v_i - v_{i-1}|. \quad (30)$$

356

357 Importantly if the solution does indeed converge to some solution then the TV must at
 358 some point plateau so that more oscillations cannot be introduced.

359 This is indeed the findings of the simulations that were run as can be seen by figure 9.
 360 With the TV increasing as Δx decreases at the start as the models resolve more and more
 361 dispersive waves. But as Δx decreases further the TV plateaus and thus the oscillations are
 362 not growing without bound. Thus the scheme has not become unstable which supports fur-
 363 ther that this formulation handles shocks and the resultant dispersive waves well. Also note
 364 that as expected the higher order the method the higher TV it has at the start and the faster
 365 it plateaus and these is very good agreement between the second and third order schemes.
 366 Although as discussed in (Zoppou and Roberts 1996) second-order schemes will produce
 367 dispersive errors and thus introduce oscillations, what this demonstrates is that such oscil-
 368 lations are so small that they are insignificant compared to the resolved oscillations by the
 369 diffusive errors of the comparable third-order scheme. Thus the move from a second- to
 370 a third-order method while resolving more of the solution doesn't demonstrate behaviour
 371 not seen in the second-order solutions.

372 **CONCLUSIONS**

373 **ACKNOWLEDGEMENTS**

374 **REFERENCES**

- 375 Carter, J. D. and Cienfuegos, R. (2011). “Solitary and cnoidal wave solutions of the serre
376 equations and their stability.” *European Journal of Mechanics B/Fluids*, 30(3), 259–268.
- 377 El, G., Grimshaw, R. H. J., and Smyth, N. F. (2006). “Unsteady undular bores in fully
378 nonlinear shallow-water theory.” *Physics of Fluids*, 18(027104).
- 379 Gottlieb, S., Ketcheson, D. I., and Shu, C. W. (2009). “High order strong stability preserving
380 time discretizations.” *Journal of Scientific Computing*, 38(3), 251–289.
- 381 Hammack, J. L. and Segur, H. (1978). “The korteweg-de vries equation and water waves.
382 part 3. oscillatory waves.” *Journal of Fluid Mechanics*, 84(2), 337–358.
- 383 Koren, B. (1993). “A robust upwind discretization method for advection, diffusion and
384 source terms.” *Notes on Numerical Fluid Mechanics*, Vol. 45, Centrum voor Wiskunde
385 en Informatica, Amsterdam.
- 386 Kurganov, A., Noelle, S., and Petrova, G. (2002). “Semidiscrete central-upwind schemes
387 for hyperbolic conservation laws and hamilton-jacobi equations.” *Journal of Scientific
388 Computing, Society for Industrial and Applied Mathematics*, 23(3), 707–740.
- 389 Lannes, D. and Bonneton, P. (2009). “*Physics of Fluids*, 21(1), 16601–16610.
- 390 Le Métayer, O., Gavrilyuk, S., and Hank, S. (2010). “A numerical scheme for the green-
391 naghdi model.” *Journal of Computational Physics*, 229(6), 2034–2045.
- 392 LeVeque, R. (2002). *Finite Volume Methods for Hyperbolic Problems*, Vol. 54 of *Cam-
393 bridge Texts in Applied Mathematics*. Cambridge University Press.
- 394 Li, M., Guyenne, P., Li, F., and Xu, L. (2014). “High order well-balanced cdg-fe methods
395 for shallow water waves by a green-naghdi model.” *Journal of Computational Physics*,
396 257, 169–192.
- 397 Su, C. H. and Gardner, C. S. (1969). “Korteweg-de vries equation and generalisations. iii.
398 derivation of the korteweg-de vries equation and burgers equation.” *Journal of Mathe-
399 matical Physics*, 10(3), 536–539.
- 400 Zoppou, C. and Roberts, S. (1996). “Behaviour of finite difference schemes for advection
401 diffusion equations.” *Technical Report Mathematics Research Report No.MRR 062-96*.

402 **NOTATION**

403 *The following symbols are used in this paper:*

- a = characteristic order of free surface amplitude;
 B = characteristic order of bottom topography variation;
 g = acceleration due to gravity on earth (m/s^2)

h_0 = characteristic water depth;
 h = water depth (m);
 L = characteristic horizontal scale;
 p = pressure (N/m^2);
 u = fluid particle velocity x -direction (m/s);
 w = fluid particle velocity z -direction (m/s);
 ϵ = nonlinearity parameter a/h_0 ;
 ξ = water depth from free surface (m) ;
 σ = shallowness parameter h_0^2/L^2 .

404 **SUBSCRIPTS**

405 i = space discretisation.

406 **SUPERSCRIPTS**

407 n = time discretisation.

408 **ACCENTS**

409 \bar{q} = quantity q averaged over the depth of water

409 \bar{q} = quantity q averaged over a Δx length interval of space [only make sense given a x position to cer

410 **List of Figures**

411 1	The notation used for one-dimensional flow governed by the Serre equation.	17
412 2	Convergence of relative error using L1 norm for analytic soliton solution for both h (○) and u (◇) for first (a), second (b) and third (c) order schemes.	18
413 3	Plotted example soliton simulation for first-order scheme (○) with $dx =$ $1.5625m$ against the analytic solution of (6) (—) with black and blue for $t = 0s$ and $t = 100s$ respectively.	19
414 4	Plotted example soliton simulation for second-order scheme (○) with $dx =$ $1.5625m$ against the analytic solution of (6) (—) with black and blue for $t = 0s$ and $t = 100s$ respectively.	20
415 5	Plotted example soliton simulation for third-order scheme (○) with $dx =$ $1.5625m$ against the analytic solution of (6) (—) with black and blue for $t = 0s$ and $t = 100s$ respectively.	21
416 6	Rectangular wave experiment for first order scheme at $\frac{x}{h_1} : 0$ (a), 50 (b), 100 (c), 150 (d) and 200 (e)	22
417 7	Rectangular wave experiment for second order scheme at $\frac{x}{h_1} : 0$ (a), 50 (b), 100 (c), 150 (d) and 200 (e)	23
418 8	Rectangular wave experiment for third order scheme at $\frac{x}{h_0} : 0$ (a), 50 (b), 100 (c), 150 (d) and 200 (e)	24
419 9	The change in total variation (TV) over Δx for first (○), second (□), and third (◇) order schemes.	25
420 10	Solutions for the dam break problem for first- (a), second- (b) and third- order (c) schemes	26
421		
422		
423		
424		
425		
426		
427		
428		
429		
430		
431		
432		

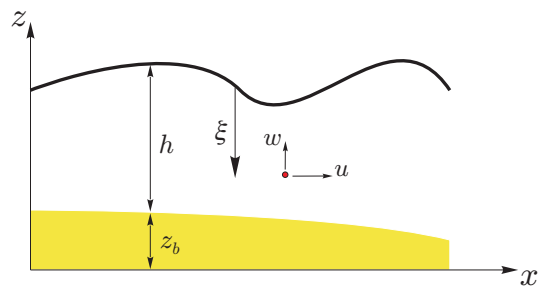


FIG. 1. The notation used for one-dimensional flow governed by the Serre equation.

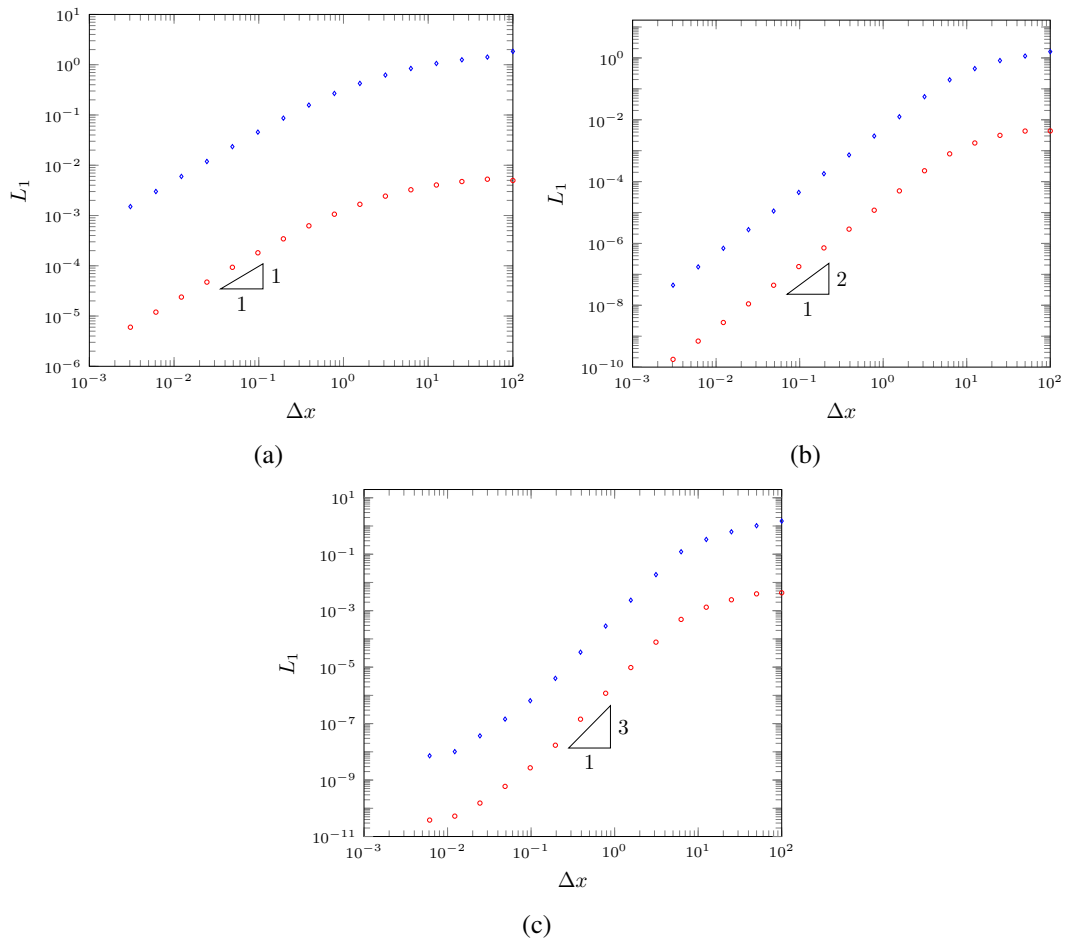


FIG. 2. Convergence of relative error using L1 norm for analytic soliton solution for both h (\circ) and u (\diamond) for first (a), second (b) and third (c) order schemes.

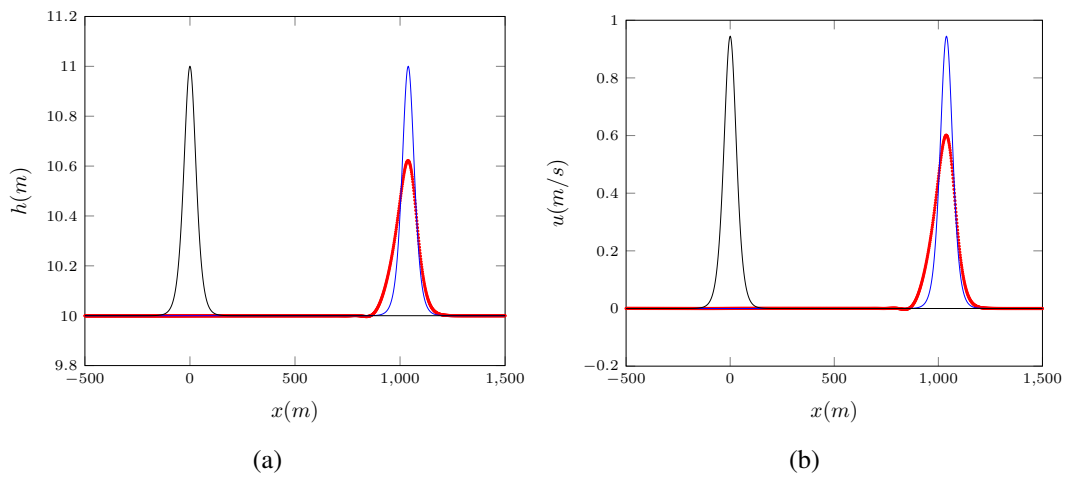


FIG. 3. Plotted example soliton simulation for first-order scheme (\circ) with $dx = 1.5625m$ against the analytic solution of (6) (—) with black and blue for $t = 0s$ and $t = 100s$ respectively.

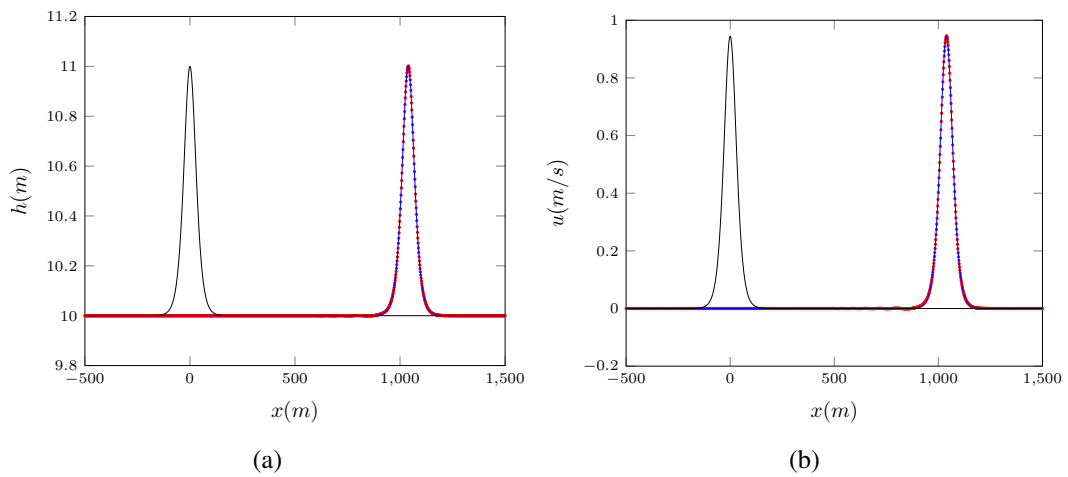


FIG. 4. Plotted example soliton simulation for second-order scheme (\circ) with $dx = 1.5625m$ against the analytic solution of (6) (—) with black and blue for $t = 0s$ and $t = 100s$ respectively.

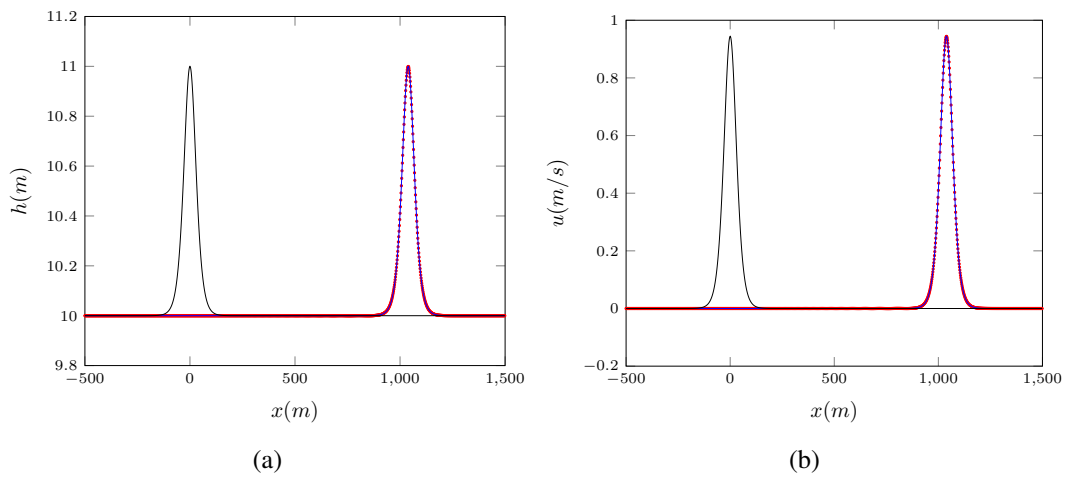


FIG. 5. Plotted example soliton simulation for third-order scheme (\circ) with $dx = 1.5625m$ against the analytic solution of (6) (—) with black and blue for $t = 0s$ and $t = 100s$ respectively.

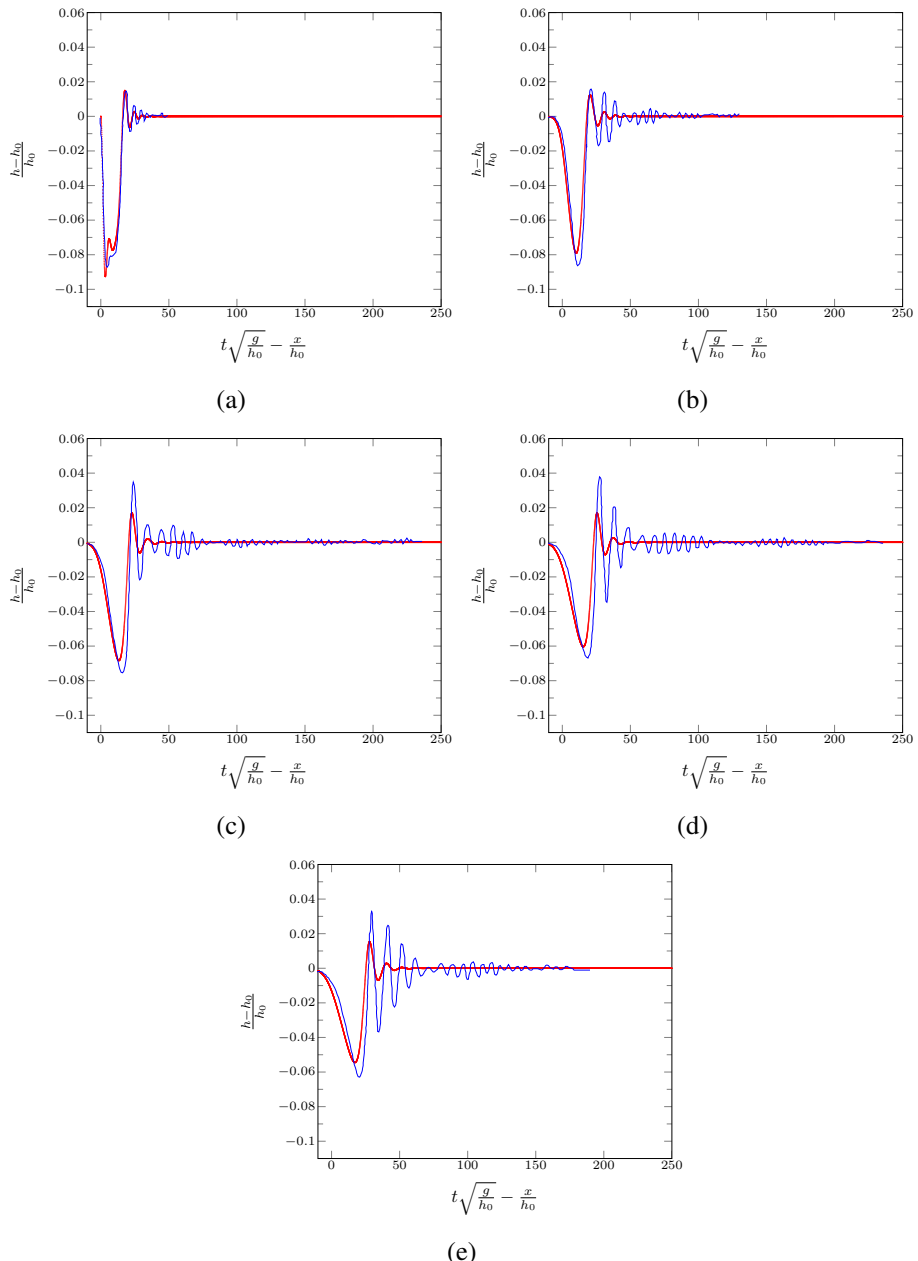


FIG. 6. Rectangular wave experiment for first order scheme at $\frac{x}{h_1} : 0$ (a), 50 (b), 100 (c), 150 (d) and 200 (e)

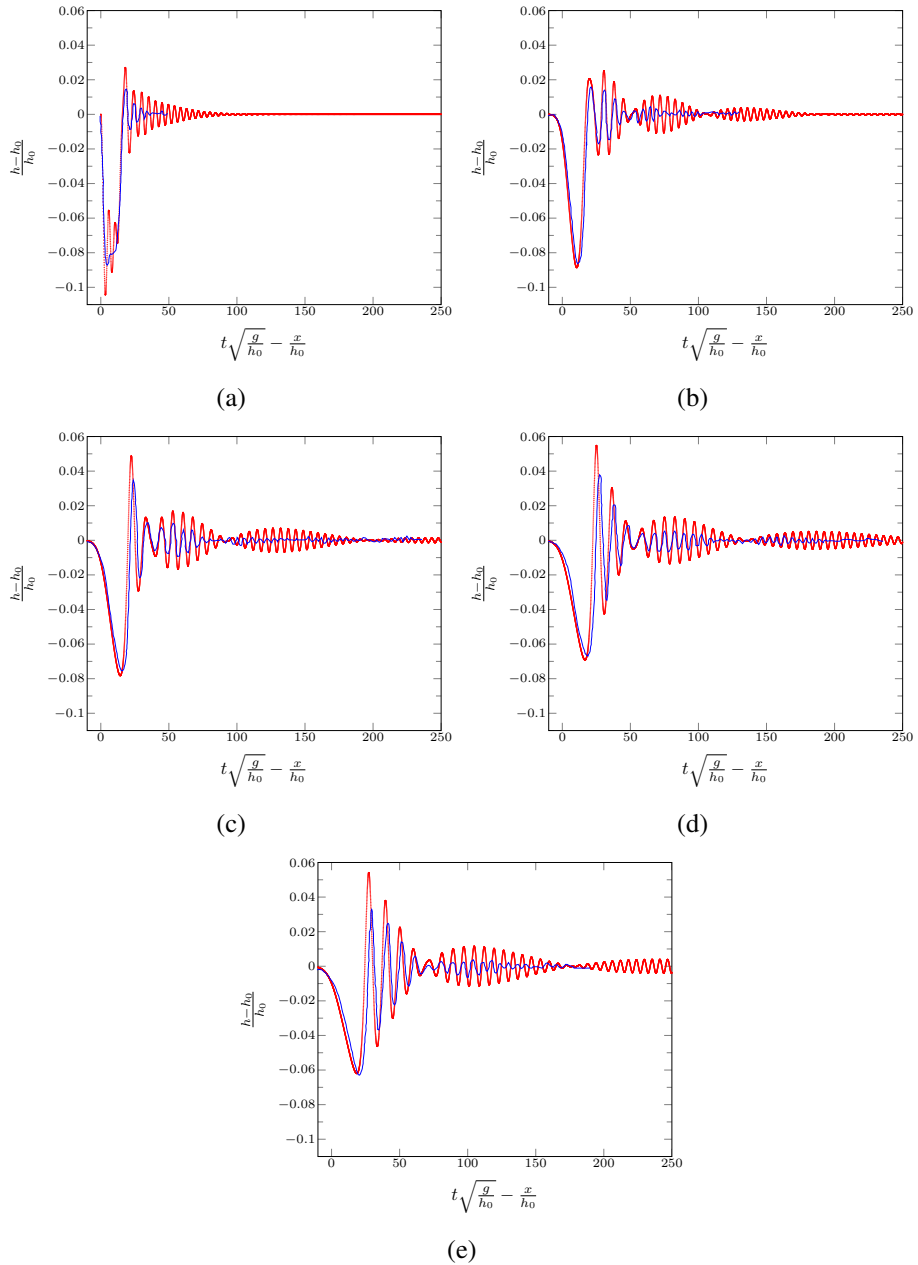


FIG. 7. Rectangular wave experiment for second order scheme at $\frac{x}{h_1} : 0$ (a), 50 (b), 100 (c), 150 (d) and 200 (e)

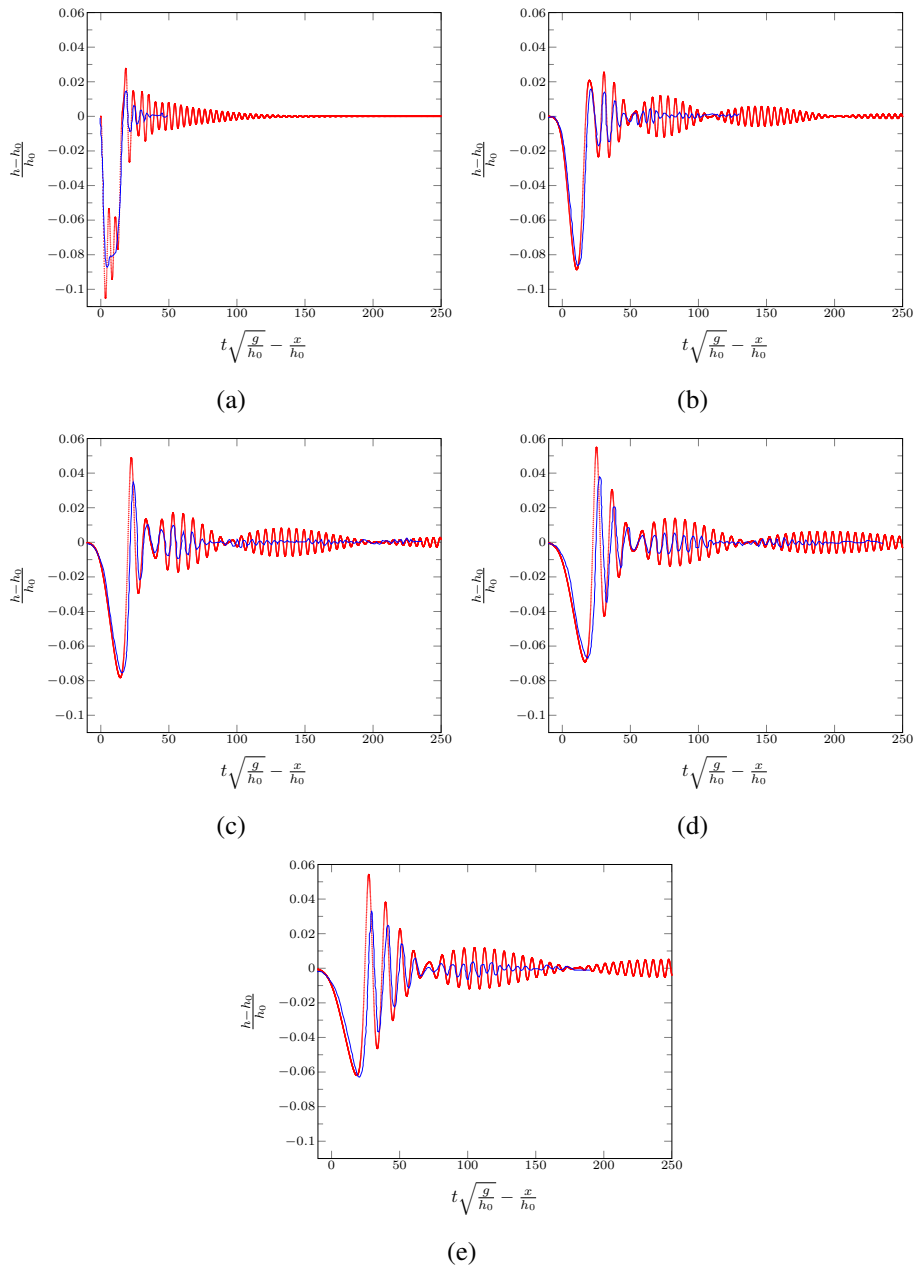


FIG. 8. Rectangular wave experiment for third order scheme at $\frac{x}{h_0} : 0$ (a), 50 (b), 100 (c), 150 (d) and 200 (e)

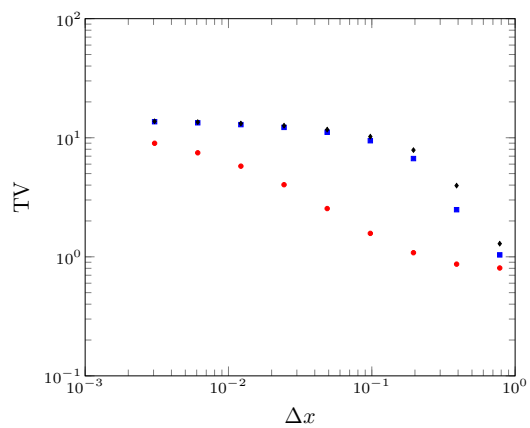


FIG. 9. The change in total variation (TV) over Δx for first (\circ) , second (\square), and third (\diamond) order schemes.

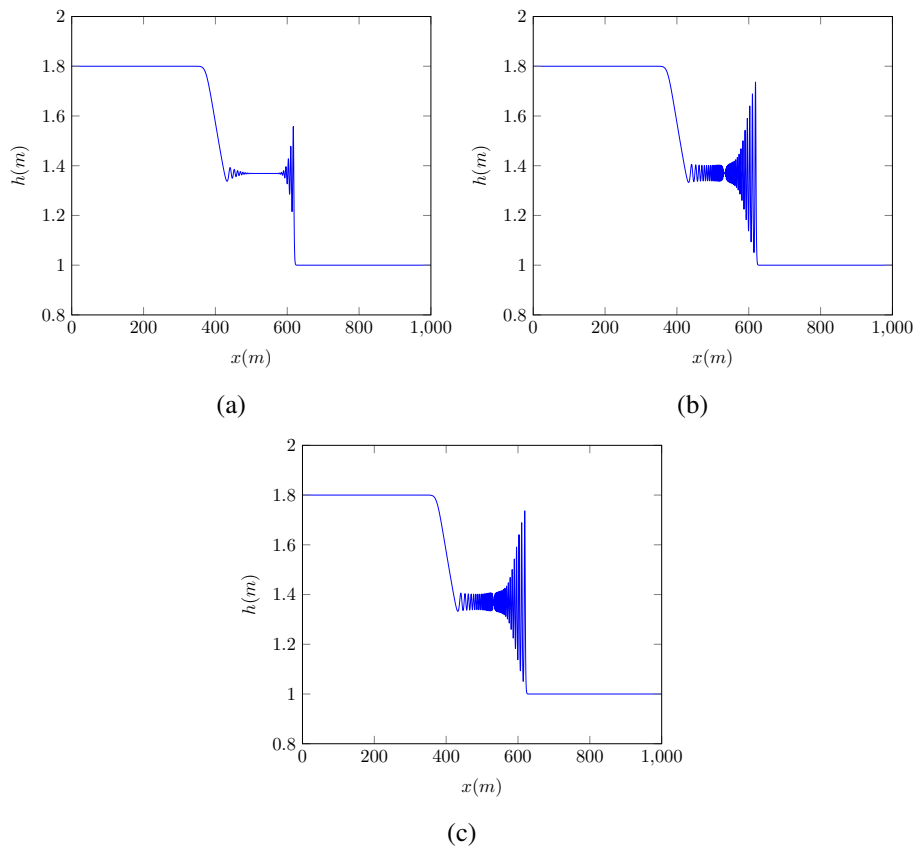


FIG. 10. Solutions for the dam break problem for first- (a), second- (b) and third-order (c) schemes